

**Phase-separating binary fluids under oscillatory shear**Aiguo Xu,<sup>1</sup> G. Gonnella,<sup>1,2</sup> and A. Lamura<sup>3</sup><sup>1</sup>*Istituto Nazionale per la Fisica della Materia, Unità di Bari, and Dipartimento di Fisica, Università di Bari, and TIRES, Center of Innovative Technologies for Signal Detection and Processing, 70126 Bari, Italy*<sup>2</sup>*INFN, Sezione di Bari, Via Amendola 173, 70126 Bari, Italy*<sup>3</sup>*Istituto Applicazioni Calcolo, CNR, Sezione di Bari, Via Amendola 122/I, 70126 Bari, Italy*

(Received 5 November 2002; published 9 May 2003)

We apply the lattice Boltzmann methods to study the segregation of binary fluid mixtures under oscillatory shear flow in two dimensions. The algorithm allows to simulate systems whose dynamics is described by the Navier-Stokes and the convection-diffusion equations. The interplay between several time scales produces a rich and complex phenomenology. We investigate the effects of different oscillation frequencies and viscosities on the morphology of the phase separating domains. We find that at high frequencies the evolution is almost isotropic with growth exponents  $2/3$  and  $1/3$  in the inertial (low viscosity) and diffusive (high viscosity) regimes, respectively. When the period of the applied shear flow becomes of the same order of the relaxation time  $T_R$  of the shear velocity profile, anisotropic effects are clearly observable. In correspondence with non-linear patterns for the velocity profiles, we find configurations where lamellar order close to the walls coexists with isotropic domains in the middle of the system. For particular values of frequency and viscosity it can also happen that the convective effects induced by the oscillations cause an interruption or a slowing of the segregation process, as found in some experiments. Finally, at very low frequencies, the morphology of domains is characterized by lamellar order everywhere in the system resembling what happens in the case with steady shear.

DOI: 10.1103/PhysRevE.67.056105

PACS number(s): 05.70.Ln, 47.20.Hw, 47.11.+j, 83.10.Tv

**I. INTRODUCTION**

The process of segregation in fluid mixtures is greatly affected by the presence of applied flows [1,2]. The domains of the separating phases generally grow with anisotropic patterns that reflect the profile of the velocity field. In the case of polymer blends subjected to a simple shear flow stringlike structures are observed aligned along the flow direction [3,4]. In more complex systems such as diblock copolymer melts with lamellar order [5] the question of the orientation of the interfaces is still a debated problem [6–8]. The presence of the flow has also less expected and obvious consequences. For example, in phase separation of binary fluids, while in the absence of flow the size of domains is distributed around a single average length scale [9], when a shear flow is applied, two typical lengths are observed for each direction [10–13]. Another peculiar case is that of lamellar sheared systems where the symmetry of dynamical scaling [9], generally holding in ordering systems, is foreseen to be violated [8]. Related to the presence of the flow is also the behavior of the stress response. The nonlinear character of this response reflects the dynamical evolution of the domain pattern and is of fundamental importance in many technological applications [14].

In this paper we study through numerical simulations the behavior of a symmetric phase separating binary mixture subjected to an oscillatory shear flow [1]. Experiments on this system show that in some cases the growth of the domains is interrupted for frequencies smaller than some critical value [15,16], while in other cases domains are observed to grow on time scales much longer than the period of a single oscillation [17]. Available simulations of this system [13,18,19] did not take into account the role of

hydrodynamics or the existence of a finite time required to set a linear shear profile in a fluid system. This time, which is inversely proportional to the viscosity in a simple fluid [20], has a very important role in the case of oscillatory shear. For example, for sufficiently high frequencies, as it will be shown later, this time is longer than the oscillation period and the linear profile will be never set in the system. This will have relevant consequences for the evolution and the morphology of the domains of the separating phases. Actually, a systematic study of the dependence of the growth properties on the frequency of oscillations has not been done in previous simulations also for the simplest cases without hydrodynamics. One has also to observe that, differently from the case with steady shear, due to the fact that the average strain is zero in one period of shearing, the effects of oscillatory shear on the morphology of domains are not always easy to understand intuitively.

The effects discussed above can be properly described only considering the full hydrodynamic equations for binary mixtures. We have used a lattice Boltzmann method (LBM) [21–23] to simulate the convection-diffusion and Navier-Stokes equations for a binary fluid. We have introduced in the lattice Boltzmann scheme, appropriate boundary conditions for a shear flow and we have run our simulations systematically changing the frequency of oscillations for a limited set of values of the viscosity. We have considered the two-dimensional case that is also useful for the comprehension of the three-dimensional case and has the advantage of being less demanding from the computational point of view.

The lattice Boltzmann simulations are based on the discretized Boltzmann equations for a set of distribution functions related to the fluid densities and velocity. The densities and momenta are conserved at each step of the simulation

thus approximating the behavior of the hydrodynamic equations for the fluid. The lattice Boltzmann methods have been found to be very convenient for simulating quasi-incompressible fluids on very long time scales, as it is needed in phase separation problems [24,25]. Another advantage of the LBM is that, in the implementation of the method used in this paper [26], a free energy can be introduced such that the fluid relaxes to the equilibrium state determined by this free energy. This allows to know accurately the equilibrium properties of the coexisting phases whose growth dynamics is under study.

Before presenting our results it is useful to summarize the known behavior of two-dimensional binary mixtures quenched into the ordered homogeneous phases in the absence of flow. Once domains of the two phases are well established, experimental and numerical data show that the growth is self-similar with the typical size of domains scaling with time as  $R(t) \sim t^\alpha$  [9]. The growth exponent  $\alpha$  depends on the physical mechanism responsible for the phase separation. A simple scaling analysis of the Navier-Stokes and of the convection-diffusion equations shows that three regimes can be found corresponding to the role played by hydrodynamic degrees of freedom [27,28]. At high viscosity the domain growth is governed by a diffusive mechanism and the growth exponent is  $\alpha = 1/3$  [29]. When hydrodynamics becomes relevant, the laws  $R(t) \sim t$  or  $R(t) \sim t^{2/3}$  are expected depending on whether viscous forces or inertial effects dominate, respectively [27,28]. In real systems, however, the situation is more complex. The physical mechanism responsible for the viscous growth is not operating in the two-dimensional case [30] and, indeed, this regime has never been observed in simulations [24].

The effects of a steady shear flow on the growth laws previously discussed have been considered in many papers. In the diffusive case, analytical calculations based on a self-consistent approximation show that the typical size of domains should grow in the direction normal to the flow as in the case without shear, while the growth exponent in the flow direction is equal to that in the transverse direction augmented of one [11,31]. This result cannot be easily checked by numerical simulations due to the presence of finite size effects that become very soon relevant in the direction of the flow affecting the value of the exponents [12]. The full problem with the Navier-Stokes and the convection-diffusion equations has been considered in Refs. [25,32–36], but also in this case reliable results for the growth exponents are not yet available. Actually, the true existence of an asymptotic growth regime in alternative with a stationary state with a finite transverse size is a question still to be clarified [37,25]. On the other hand, morphological properties are reasonably well understood. Domains are stretched by the flow and this induces a coagulation of domains in the flow direction but also ruptures in the bicontinuous network [12,38]. As a result, domains assume the typical stringlike character with the already mentioned complication that the size of domains is distributed around two typical length scales for each direction.

The lattice Boltzmann scheme used in this paper is described in the following section. Due to small variations with

respect to previous LBM [39], details on the method and on the implementation are given for convenience of the reader. The rest of the paper is divided as follows. In Sec. III, we illustrate our strategy for the choice of the parameters used in the simulations; we also discuss the relevant time scales for the system considered. In Sec. IV, we show results of simulations where the growth is dominated by inertial effects, while the diffusive case is treated in Sec. V. In Sec. VI, we consider the behavior of the shear stress, and we draw our conclusions in Sec. VII.

## II. THE MODEL

Our simulations are based on the lattice Boltzmann scheme developed by Orlandini *et al.* [39] and Swift *et al.* [40]. In this scheme the equilibrium properties of the system can be controlled by introducing a free energy which enters properly into the lattice Boltzmann model.

### A. The lattice Boltzmann scheme

The lattice Boltzmann scheme is based on the  $D2Q9$  lattice: A square lattice is used in which each site is connected with nearest and next-to-nearest neighbors. The horizontal and vertical links have length  $\Delta x$ , the diagonal links  $\sqrt{2}\Delta x$ ,  $\Delta x$  being the space step. Two sets of distribution functions  $f_i(\mathbf{r}, t)$  and  $g_i(\mathbf{r}, t)$  are defined on each lattice site  $\mathbf{r}$  at each time  $t$ . Each of them is associated with a velocity vector  $\mathbf{e}_i$ . Defined  $\Delta t$  as the simulation time step, the quantities  $\mathbf{e}_i \Delta t$  are constrained to be lattice vectors so that  $|\mathbf{e}_i| = \Delta x / \Delta t \equiv c$  for  $i = 1$  (east direction), 2 (north), 3 (west), 4 (south) and  $|\mathbf{e}_i| = \sqrt{2}c$  for  $i = 5$  (north east), 6 (north west), 7 (south west), 8 (south east). Two functions  $f_0(\mathbf{r}, t)$  and  $g_0(\mathbf{r}, t)$ , corresponding to the distribution components that do not propagate ( $\mathbf{e}_0 = \mathbf{0}$ ), are also taken into account. They evolve during the time step  $\Delta t$  according to a single relaxation-time Boltzmann equation [41,42]:

$$f_i(\mathbf{r} + \mathbf{e}_i \Delta t, t + \Delta t) - f_i(\mathbf{r}, t) = -\frac{1}{\tau} [f_i(\mathbf{r}, t) - f_i^{eq}(\mathbf{r}, t)], \quad (1)$$

$$g_i(\mathbf{r} + \mathbf{e}_i \Delta t, t + \Delta t) - g_i(\mathbf{r}, t) = -\frac{1}{\tau_\varphi} [g_i(\mathbf{r}, t) - g_i^{eq}(\mathbf{r}, t)], \quad (2)$$

where  $\tau$  and  $\tau_\varphi$  are independent relaxation parameters, and  $f_i^{eq}(\mathbf{r}, t)$  and  $g_i^{eq}(\mathbf{r}, t)$  are local equilibrium distribution functions. The distribution functions are related to the total density  $n$ , to the fluid momentum  $n\mathbf{v}$ , and to the density difference  $\varphi$ , through

$$n = \sum_i f_i, \quad n\mathbf{v} = \sum_i f_i \mathbf{e}_i, \quad \varphi = \sum_i g_i. \quad (3)$$

These quantities are locally conserved in any collision process and, therefore, we require that the local equilibrium distribution functions fulfill the equations

$$\sum_i (f_i^{eq} - f_i) = 0 \Rightarrow \sum_i f_i^{eq} = n,$$

$$D_I = 4D_{II}, \quad D_{II} = \frac{n}{8c^4}, \quad (12)$$

$$\sum_i (g_i^{eq} - g_i) = 0 \Rightarrow \sum_i g_i^{eq} = \varphi,$$

$$G_{I,\alpha\beta} = 4G_{II,\alpha\beta}, \quad G_{II,\alpha\beta} = \frac{P_{\alpha\beta} - \frac{1}{2}P_{\sigma\sigma}\delta_{\alpha\beta}}{8c^2}. \quad (13)$$

$$\sum_i (f_i^{eq} - f_i)\mathbf{e}_i = \mathbf{0} \Rightarrow \sum_i f_i^{eq}\mathbf{e}_i = n\mathbf{v}. \quad (4)$$

Following Refs. [39,40], the higher moments of the local equilibrium distribution functions are defined so that the continuum equations pertinent to a binary fluid mixture can be obtained and the equilibrium thermodynamic properties of the system can be controlled. We define

$$\sum_i f_i^{eq} e_{i\alpha} e_{i\beta} = c^2 P_{\alpha\beta} + n v_\alpha v_\beta, \quad (5)$$

$$\sum_i g_i^{eq} e_{i\alpha} = \varphi v_\alpha, \quad (6)$$

$$\sum_i g_i^{eq} e_{i\alpha} e_{i\beta} = c^2 \Gamma \Delta\mu \delta_{\alpha\beta} + \varphi v_\alpha v_\beta, \quad (7)$$

where  $P_{\alpha\beta}$  is the pressure tensor,  $\Delta\mu$  is the chemical potential difference between the two fluids, and  $\Gamma$  is a coefficient related to the mobility of the fluid. We want to stress that we are considering a mixture with the two fluids having the same mechanical properties and, in particular, the same viscosity. Constraint (6) expresses the fact that the two fluids have the same velocity. The local equilibrium distribution functions can be expressed as an expansion at the second order in the velocity  $\mathbf{v}$  [39,40]:

$$f_0^{eq} = A_0 + C_0 v^2,$$

$$f_i^{eq} = A_I + B_I v_\alpha e_{i\alpha} + C_I v^2 + D_I v_\alpha v_\beta e_{i\alpha} e_{i\beta} + G_{I,\alpha\beta} e_{i\alpha} e_{i\beta}, \quad i = 1, 2, 3, 4,$$

$$f_i^{eq} = A_{II} + B_{II} v_\alpha e_{i\alpha} + C_{II} v^2 + D_{II} v_\alpha v_\beta e_{i\alpha} e_{i\beta} + G_{II,\alpha\beta} e_{i\alpha} e_{i\beta}, \quad i = 5, 6, 7, 8, \quad (8)$$

and similarly for the  $g_i^{eq}$ ,  $i = 0, \dots, 8$ . Relations (4) and (5) can be used to fix the coefficients of these expansions. A suitable choice of the coefficients in expansions (8) is

$$A_0 = n - 20A_{II}, \quad A_I = 4A_{II}, \quad A_{II} = \frac{P_{\alpha\beta}\delta_{\alpha\beta}}{24}, \quad (9)$$

$$B_I = 4B_{II}, \quad B_{II} = \frac{n}{12c^2}, \quad (10)$$

$$C_0 = -\frac{2n}{3c^2}, \quad C_I = 4C_{II}, \quad C_{II} = -\frac{n}{24c^2}, \quad (11)$$

The expansion coefficients for the  $g_i^{eq}$  can be obtained from the previous ones with the formal substitutions  $n \rightarrow \varphi$  and  $P_{\alpha\beta} \rightarrow \Gamma \Delta\mu \delta_{\alpha\beta}$ . The quantities  $P_{\alpha\beta}$  and  $\Delta\mu$ , which appear in the coefficients of the equilibrium distribution functions, can be calculated from a suitable free energy.

## B. The equilibrium properties

The free-energy functional used in the present study is

$$\mathcal{F} = \int d\mathbf{r} \left[ \frac{1}{3} n \ln n + \frac{a}{2} \varphi^2 + \frac{b}{4} \varphi^4 + \frac{\kappa}{2} (\nabla \varphi)^2 \right]. \quad (14)$$

The term in  $n$  gives rise to a positive background pressure and does not affect the phase behavior; it is required in the lattice Boltzmann approach, as it will be seen later. The terms in  $\varphi$  in the free-energy density  $f(n, \varphi)$  correspond to the usual Ginzburg-Landau free energy typically used in studies of phase separation [28]. The polynomial terms are related to the bulk properties of the fluid. While the parameter  $b$  is always positive, the sign of  $a$  distinguishes between a disordered ( $a > 0$ ) and a segregated mixture ( $a < 0$ ), where two pure phases with  $\varphi = \pm \sqrt{-a/b}$  coexist. We will consider quenches into the coexistence region with  $a < 0$  and  $b = -a$  so that the equilibrium values for the order parameter are  $\varphi = \pm 1$ . The gradient term is related to the interfacial properties. The equilibrium profile between the two coexisting bulk phases is  $\varphi(x) = \tanh 2x/\xi$  giving [43] a surface tension

$$\sigma = \frac{2}{3} \sqrt{-2a\kappa} \quad (15)$$

and an interfacial width

$$\xi = 2 \sqrt{\frac{2\kappa}{-a}}. \quad (16)$$

The thermodynamic properties of the fluid follow from the free energy (14). The chemical potential difference between the two fluids is given by

$$\Delta\mu = \frac{\delta\mathcal{F}}{\delta\varphi} = a\varphi + b\varphi^3 - \kappa \nabla^2 \varphi. \quad (17)$$

The pressure is a tensor  $P_{\alpha\beta}$  since interfaces in the fluid can exert nonisotropic forces [44]. The diagonal part  $p_o$  can be calculated from Eq. (14) by using thermodynamics relations,

$$p_o = n \frac{\delta \mathcal{F}}{\delta n} + \varphi \frac{\delta \mathcal{F}}{\delta \varphi} - f(n, \varphi) = \frac{1}{3}n + \frac{a}{2}\varphi^2 + \frac{3b}{4}\varphi^4$$

$$- \kappa \varphi (\nabla^2 \varphi) - \frac{\kappa}{2} (\nabla \varphi)^2. \quad (18)$$

In deriving the pressure tensor  $P_{\alpha\beta}$ , one has to ensure that  $P_{\alpha\beta}$  obeys the condition of mechanical equilibrium  $\partial_\alpha P_{\alpha\beta} = 0$  [45]. A suitable choice is

$$P_{\alpha\beta} = p_o \delta_{\alpha\beta} + \kappa \partial_\alpha \varphi \partial_\beta \varphi. \quad (19)$$

The presence of the term depending on  $n$  in the free-energy density allows to recover the known results of the  $D2Q9$  lattice Boltzmann model for a single fluid. Indeed, when  $a = b = \kappa = \varphi = 0$ , expansion coefficients (9)–(13) become those of the  $D2Q9$  model [46] and the pressure tensor (19) reduces to the scalar  $p = (c^2/3)n$ , where we have also included the factor  $c^2$  appearing in the rhs of Eq. (5). This is the pressure for an ideal gas with speed of sound  $c_s = c/\sqrt{3}$  [46]. Let us observe that the value of the numerical factor in front of  $n \ln n$  in the free energy depends on the topology of the lattice and the spatial dimensions [47].

It has been shown in Refs. [39,40], using a Chapman-Enskog expansion [48], that the above described lattice Boltzmann scheme simulates, at second order in  $\Delta t$ , the continuity, the quasi-incompressible Navier-Stokes, and the convection-diffusion equations with the kinematic viscosity  $\nu$  and the macroscopic mobility  $\Theta$  given by

$$\nu = \Delta t \frac{c^2}{3} (\tau - \frac{1}{2}), \quad \Theta = \Gamma \Delta t c^2 (\tau_\varphi - \frac{1}{2}). \quad (20)$$

### C. The shear boundary condition

In order to enforce a shear flow on the system, we have used the following scheme. We assume that the shear flow is directed along the horizontal direction. Boundary walls are placed on the upper and lower rows of sites. Let us consider the upper wall (similar considerations apply to the lower wall). After the propagation the distribution functions  $f_0(t)$ ,  $f_1(t)$ ,  $f_5(t)$ ,  $f_2(t)$ ,  $f_6(t)$ , and  $f_3(t)$  are known on each site, while  $f_7(t)$ ,  $f_4(t)$ ,  $f_8(t)$  are not. One uses Eqs. (3) to determine them as well as  $n$ . Requiring that the wall velocities  $w_{x,t} = \gamma_0(L-1)/2\cos(2\pi ft)$ ,  $w_{y,t} = 0$  are imposed to the fluid, we can write

$$f_7(t) + f_4(t) + f_8(t) = n - [f_0(t) + f_1(t) + f_5(t) + f_2(t) + f_6(t) + f_3(t)],$$

$$f_8(t) - f_7(t) = n \gamma_0 \frac{L-1}{2c} \cos(2\pi ft) - [f_1(t) - f_3(t) + f_5(t) - f_6(t)],$$

$$f_7(t) + f_4(t) + f_8(t) = f_5(t) + f_2(t) + f_6(t), \quad (21)$$

where  $L$  is the lattice size,  $\gamma_0$  is the amplitude of the shear rate, and  $f$  is the frequency of the oscillatory shear. Consistency of Eqs. (21) gives

$$n = f_0(t) + f_1(t) + f_3(t) + 2[f_2(t) + f_6(t) + f_5(t)]. \quad (22)$$

The system of Eqs. (21) reduces to two equations with three unknown variables. To close the system of equations the bounceback rule [49,50] is adopted for the distribution functions normal to the boundary. This corresponds to imposing that  $f_4(t) = f_2(t)$ . In order to preserve correctly mass conservation we add a further constraint. Mass will be conserved if the total density  $n$  on each site is equal to the quantity  $\hat{n}$  given by the sum

$$\hat{n}(t, t - \Delta t) = f_0(t - \Delta t) + f_5(t - \Delta t) + f_2(t - \Delta t) + f_6(t - \Delta t),$$

$$+ f_1(t) + f_5(t) + f_2(t) + f_6(t) + f_3(t), \quad (23)$$

where quantities at time  $(t - \Delta t)$  refer to the previous time step and have not been propagated over the lattice. In order to impose the constraint that on all the boundary sites  $n = \hat{n}$ , we have to introduce an independent variable in the system of equations. We have chosen  $f_0(t)$  since it does not propagate [34]. The solutions of the system of Eqs. (21) and  $n = \hat{n}$  are

$$f_0(\mathbf{r}, t) = \hat{n} - [f_1(\mathbf{r}, t) + f_3(\mathbf{r}, t)] - 2[f_2(\mathbf{r}, t) + f_5(\mathbf{r}, t) + f_6(\mathbf{r}, t)],$$

$$f_4(\mathbf{r}, t) = f_2(\mathbf{r}, t),$$

$$f_8(\mathbf{r}, t) = f_6(\mathbf{r}, t) - \frac{1}{2}[f_1(\mathbf{r}, t) - f_3(\mathbf{r}, t)] + \frac{1}{2}n\gamma_0 \frac{L-1}{2c} \cos(2\pi ft),$$

$$f_7(\mathbf{r}, t) = f_5(\mathbf{r}, t) + \frac{1}{2}[f_1(\mathbf{r}, t) - f_3(\mathbf{r}, t)] - \frac{1}{2}n\gamma_0 \frac{L-1}{2c} \cos(2\pi ft). \quad (24)$$

A similar treatment is required for the  $g_i(\mathbf{r}, t)$ . With this choice the proper momentum at the boundary is achieved. At this point the collision step is applied to all sites, including the boundary ones. By this procedure, once the system has been initialized, the application of the propagation and collision steps goes on preserving mass and momentum conservations and implementing the correct velocity values on the boundaries, as it has also been verified numerically [34].

Finally, we also require that the two fluids, which, as already stated, are assumed to have the same dynamic and static properties, have a neutral wetting with walls. This can be enforced at each time step by the condition

TABLE I. Parameters used in simulations and corresponding time scales. The shear time scale  $T_S$  is equal in all runs to 200.

Set	$\Delta t$	$T_R$	$T_D$	$T_0$	$-a, b$	$k$	$\tau$	$\Gamma$	$\sigma$
1	0.2	189720	1224.8	4815.8	$1.252 \times 10^{-4}$	$8 \times 10^{-5}$	0.5210	40	$9.43 \times 10^{-5}$
2	0.2	25638	1224.8	$1.95 \times 10^6$	$1.252 \times 10^{-4}$	$8 \times 10^{-5}$	0.6554	40	$9.43 \times 10^{-5}$
3	0.2	2563.8	1224.8	$1.95 \times 10^9$	$1.252 \times 10^{-4}$	$8 \times 10^{-5}$	2.0540	40	$9.43 \times 10^{-5}$
4	1	13280	5895.5	2024.9	$1.042 \times 10^{-2}$	$6.67 \times 10^{-3}$	2	0.5	$7.86 \times 10^{-3}$
5	1	13280	7863.4	3599.9	$7.813 \times 10^{-3}$	$5 \times 10^{-3}$	2	0.5	$5.89 \times 10^{-3}$

$$\mathbf{m} \cdot \nabla \varphi = 0, \tag{25}$$

where  $\mathbf{m}$  is a unit vector normal to the wall [51,52]. This corresponds to fixing the gradient of the density  $\varphi$  on the walls so that the angle formed by the interfaces between the two fluids with the walls stays at a constant value of  $\pi/2$  rad. This completes the description of the model used in the present work.

### III. PARAMETER SELECTION AND RELEVANT TIME SCALES

We have studied the effects of the applied flow by changing the frequency of the oscillations at fixed values of the parameters  $a, b, \kappa, \tau, \Gamma$ . This has been systematically done for the cases reported in Table I. We have kept the ratio  $\kappa/a$  fixed in such a way that the interfacial width is always of about 3 lattice spacings. We fixed  $\tau_\varphi = 1$  with  $\Gamma$  controlling

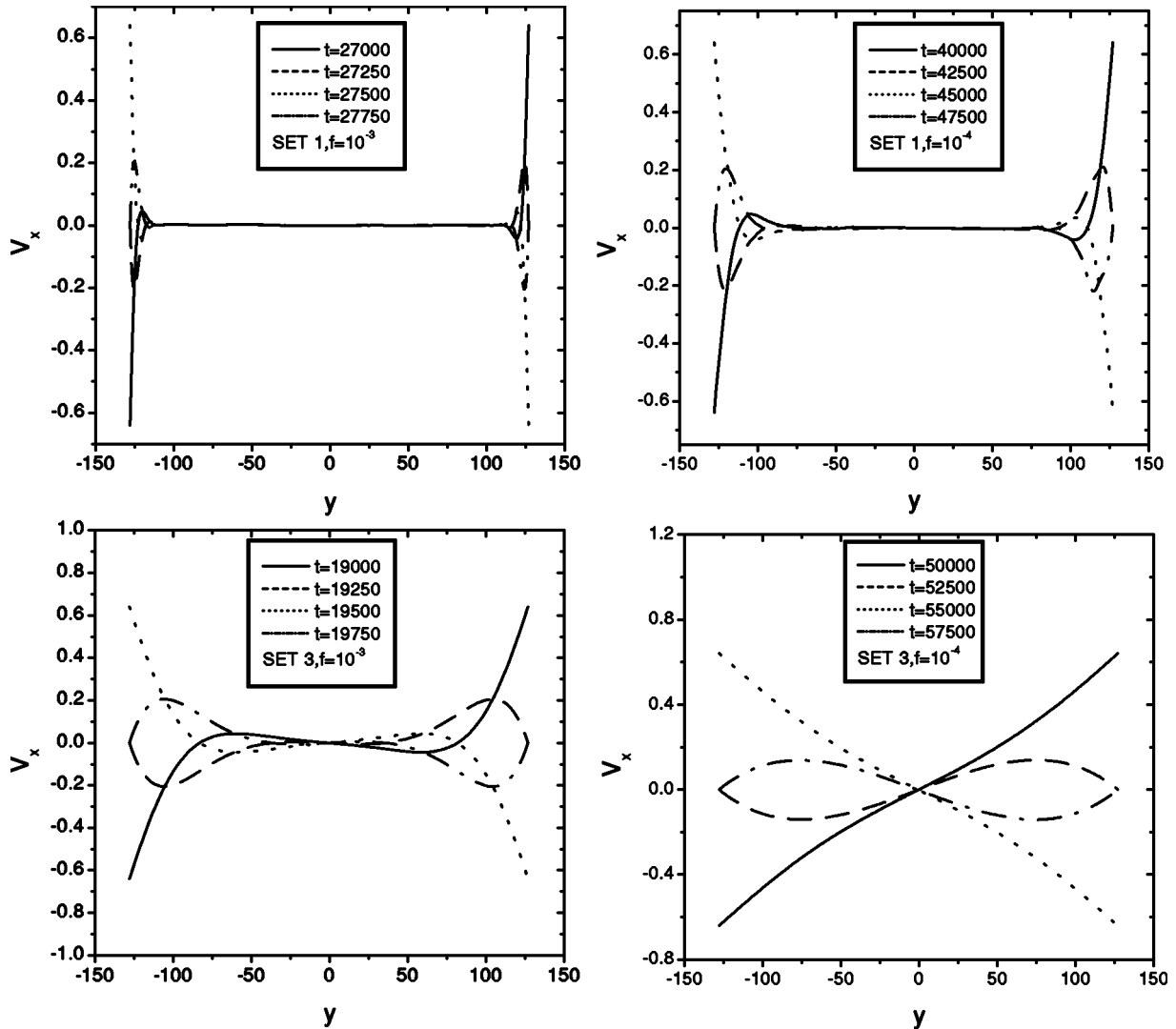


FIG. 1. Horizontal velocity profiles taken at the central vertical line of the system. The profiles are recorded at the beginning, half, first, and third quarters of the period considered.

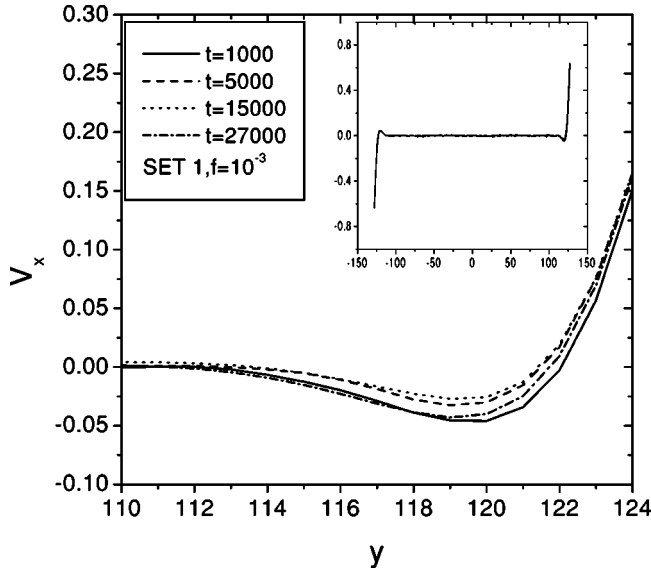


FIG. 2. The evolution of the horizontal profile for the case and at the times reported in the inset. The main frame is a magnification of the profiles in the region close to the upper wall.

the value of the macroscopic mobility (20). The amplitude of the shear rate is equal in all runs to the value  $\gamma_0 = 0.005$ . The size of the lattice, if not otherwise stated, is  $L = 256$ . In the following all the quantities are measured in units of  $\Delta x$  and  $\Delta t$ .

In the absence of shear, as observed in Refs. [25,53], the behavior at late times of a viscous phase separating binary mixture can be described in terms of adimensional temporal and spatial quantities. Indeed, from the set of macroscopic parameters  $n, \sigma, \nu$ , it is possible to define only one unit of length ( $L_0 = n\nu^2/\sigma$ ) and one of time ( $T_0 = n^2\nu^3/\sigma^2$ ).<sup>1</sup> Then, in a regime of dynamical scaling with the size of domains distributed around a single typical length, when diffusion is negligible, it is possible to build up only one spatial and one temporal adimensional variables. These variables have been used in comparing results of simulations performed with different parameters and methods [25,53].

The same use of adimensional variables can be done in the case of very high viscosity when the evolution equations reduce to a convection-diffusion equation.  $T_D = \xi^3/(\Theta\sigma)$  is the time scale for diffusion [28].

In the case with oscillatory shear the situation is more complex because various temporal scales can be defined and, in general, one does not expect dynamical scaling. Due to these reasons we have preferred to show our results in terms of original quantities. However, it remains useful to consider the relevant time scales because they can give informations on the physical mechanisms responsible of phase separation and on the role of the applied flow.

We have already defined the quantities  $T_0$  and  $T_D$  which do not depend on the applied flow. Then there are the time  $T_S = \gamma_0^{-1}$ , related to the amplitude of the oscillating shear,

<sup>1</sup>These expressions do not depend on the spatial dimension.

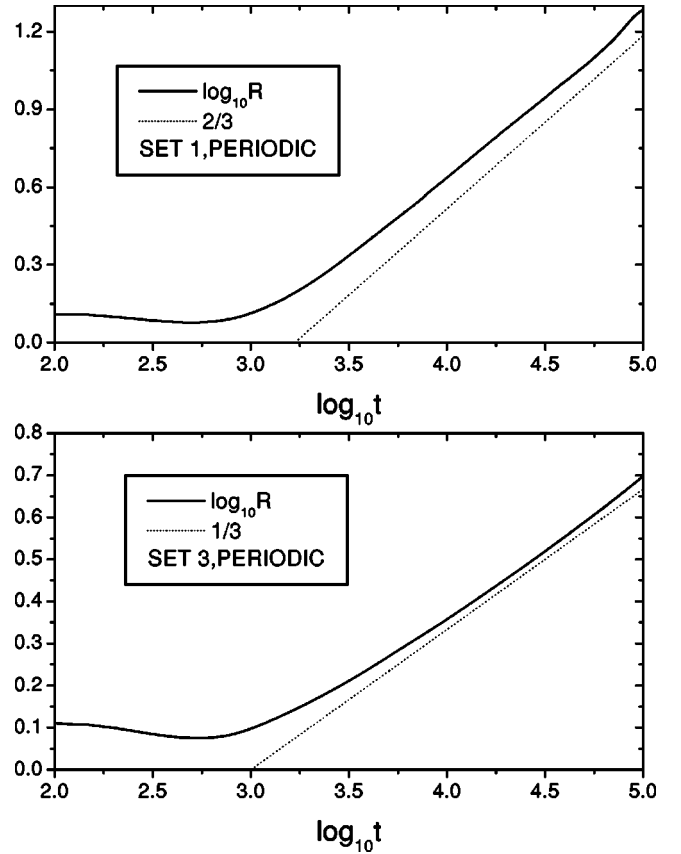


FIG. 3. Evolution of the domain size in cases without applied flow with periodic boundary conditions. The size of the lattice used in these simulations is  $L = 512$ .

and the period  $T = f^{-1}$  of a single oscillation. The ratio  $T_0/T_S$  can be interpreted as an indicator of the relative relevance of hydrodynamic and imposed velocities. Finally, we consider the quantity  $T_R = L^2/(\nu\pi^2)$  which is the leading contribution to the relaxation time for a steady shear profile in a simple fluid [20]. This time can be taken as indicative of the relaxational velocity processes also in the case of a phase separating binary mixture [34]. In Table I the time scales corresponding to the sets of parameters indicated are also reported.

The relevance of the ratio  $T_R/T$  for the problem considered in this paper appears clearly from Fig. 1. Here the horizontal velocity  $v_x$  profiles for the vertical cross section in the middle of the system are reported at a late stage of simulations for cases 1 and 3 of Table I and for two different frequencies. We checked that these results are independent of the particular vertical line considered. For each case the velocity profile is plotted at the quarters of one period. For the set of parameters 1 with  $f = 10^{-3}$  the horizontal velocity induced by the shear is very small in the bulk of the system and comparable with the average of the modulus of the vertical velocity  $v_y$ . With the same parameters, when the frequency decreases to  $f = 10^{-4}$ , the complex nonmonotonic behavior of the horizontal velocity is more evident.  $v_x$  is much larger than hydrodynamic velocities in a relevant portion of the system close to the walls where it also assumes

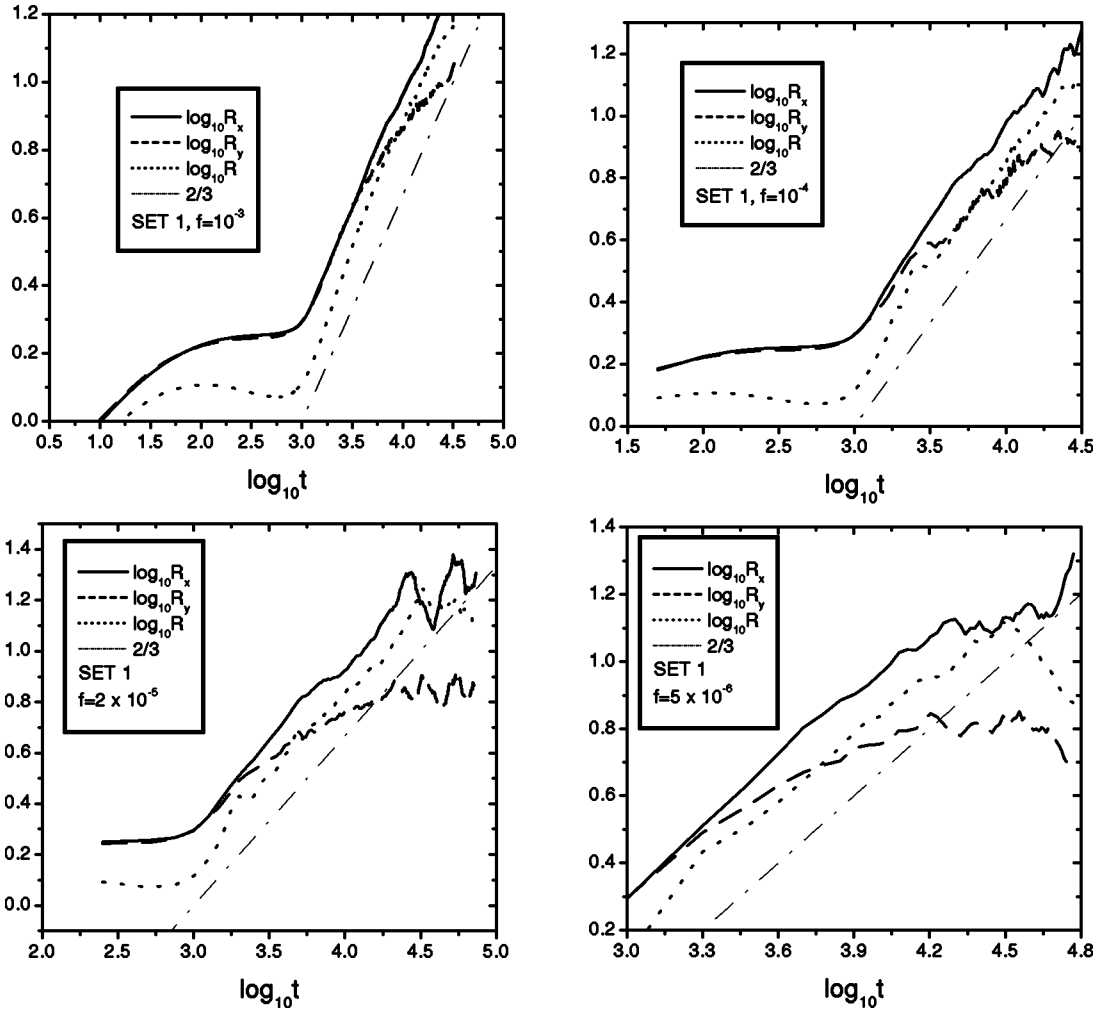


FIG. 4. Evolution of the horizontal, vertical, and spherically averaged size of domains in double logarithmic scale. The straight dashed lines have the slope written in the insets.

opposite directions to those imposed by the walls. This peculiar pattern of the velocity profiles has consequences for the behavior of the stress, as it will be seen later. When the viscosity becomes higher, like for the other set of parameters used in Fig. 1, the relaxation time  $T_R$  decreases. Then, for the same frequencies, the velocity in the bulk of the system is larger and almost triangular oscillating profiles can be observed at  $f=10^{-4}$ . We have also checked that each set of four profiles of Fig. 1 is typical for the parameters considered in the sense that only small variations in the pattern of these profiles, probably due to the evolving interface configuration, can be observed during the simulation. Figure 2 shows the velocity profile at the same phase of four different periods at initial and late stages of the simulation with set 1 of parameters at  $f=10^{-3}$ . Small quantitative changes can be observed in the region close to the walls, while the general shape of the profile always remains the same.

Finally, we consider the question of the stability of the lattice Boltzmann scheme used in this work. As observed in Ref. [53], this lattice Boltzmann scheme is intrinsically unstable. At unpredictable times of the simulation pressure waves grow up indefinitely in very few iterations making not possible the continuation of the simulation. As expected, we

saw that this problem becomes more serious when  $\tau$  tends to the limit  $1/2$ . The problem of stability is connected to that of guaranteeing as much as possible the incompressibility of the fluid. Compressibility errors, which go like  $(v/c_s)^2$  [54], can be reduced by either increasing  $c_s$ , which would require to reduce  $\Delta t$ , or decreasing the magnitude of  $a, b, \kappa$  [53]. We have followed a mixed strategy by keeping  $\Delta x=1$  and changing the values of  $\Delta t$  as reported in Table I. In this way we were able to run simulations long enough to study the phase separation of binary mixtures in different growth regimes implicitly assuming that the evolution of the system is not affected by the possible occurrence of the numerical instability. A comment to the results of Ref. [53] is that the introduction of walls for the shear boundary conditions makes worst the stability properties of the LB scheme.

#### IV. INERTIAL ORDERING

In two-dimensional quiescent systems, as discussed in the Introduction, two growth regimes with different power-law behaviors for the average size of domains  $R(t)$  have been

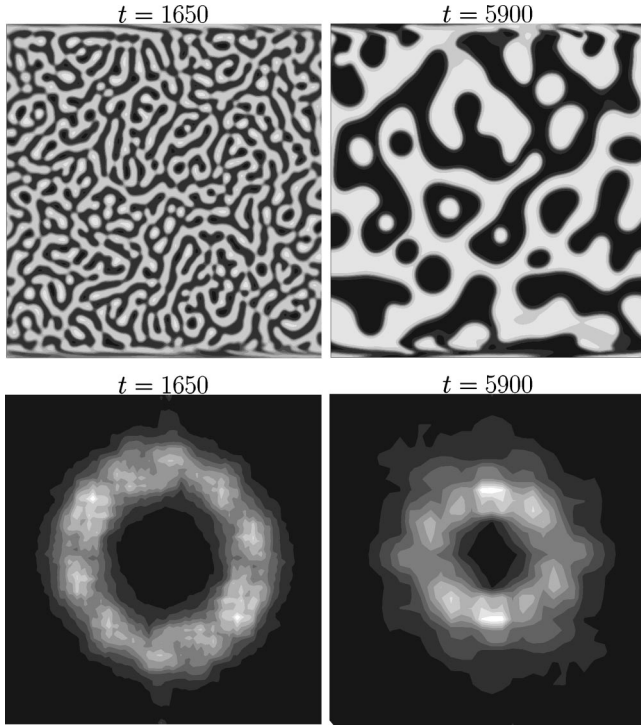


FIG. 5. Configuration of domains with the corresponding structure factor at two times in a run with parameter set 1 of parameters at the frequency  $f=10^{-3}$ . The variables  $k_x$  (horizontal axis) and  $k_y$  (vertical axis) vary in the interval  $[-5/16\pi, 5/16\pi]$  and  $[-\pi/8, \pi/8]$  at times  $t=1650$  and  $t=5900$ , respectively.

clearly identified.<sup>2</sup> In this section we will consider the effects of the oscillatory shear on the case of phase separation driven by inertial growth. We will mostly refer to case 1 of Table I for which, in the absence of flow, the behavior of  $R(t)$  is shown in Fig. 3. The quantity  $R(t)$  has been calculated as the first momentum of the structure factor, that is,

$$R(t) = \frac{\int dk C(k, t)}{\int dk k C(k, t)}, \quad (26)$$

where  $C(k, t)$  is the spherical average of the structure factor

$$C(\vec{k}, t) = \langle \varphi(\vec{k}, t) \varphi(-\vec{k}, t) \rangle, \quad (27)$$

and  $\langle \cdot \rangle$  is the average over different histories. We found a growth exponent  $\alpha = 0.62 \pm 0.02$ ;<sup>3</sup> in the following, all the estimates of the growth exponent  $\alpha$  are affected by the same error  $\pm 0.02$ . The small discrepancy from the expected value  $\alpha = 2/3$  typical for the inertial growth can be attributed to a small violation of dynamical scaling [55].

<sup>2</sup>Growth regimes with exponent 1/2 have also been reported; their existence at asymptotic times is still under debate. For a discussion, see, Ref. [24].

<sup>3</sup>For a more accurate measure of this exponent we have used larger lattices with  $L=512$ .

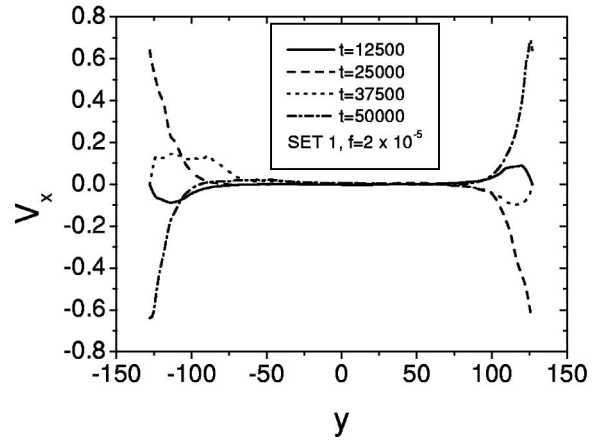
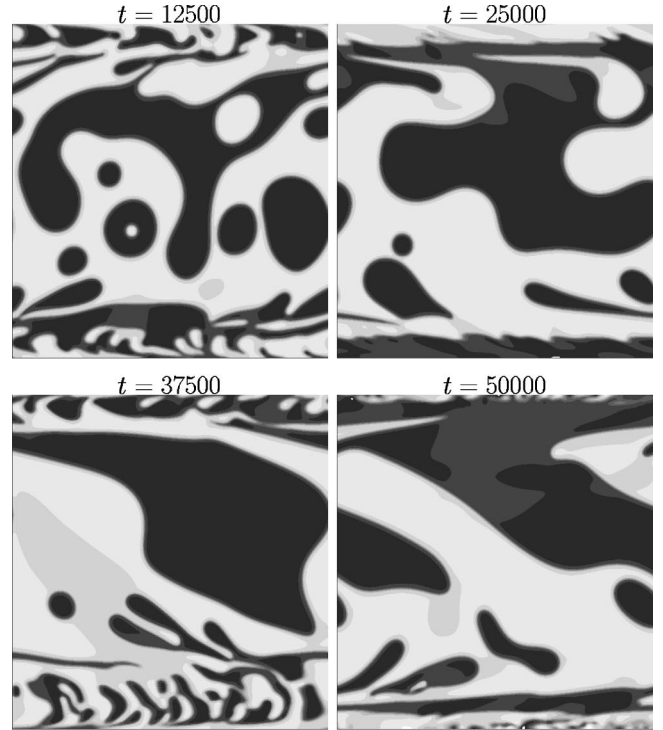


FIG. 6. Four configurations and corresponding velocity profiles in a run with period  $T=50000$ .

The effects of the oscillatory shear on the growth of the domain size for case 1 of Table I can be seen in the panel of Fig. 4 which summarizes our results for a range of frequencies from  $f=10^{-3}$  up to  $f=5 \times 10^{-6}$ . We measure the spherical average  $R(t)$ , the domain size in the flow direction

$$R_x(t) = \frac{\int d\vec{k} C(\vec{k}, t)}{\int d\vec{k} |k_x| C(\vec{k}, t)} \quad (28)$$

and the analog  $R_y$  for the shear direction. The value  $f=10^{-3}$  is the highest frequency where an anisotropic behavior can be observed.  $R$  and  $R_x$  evolve with an exponent which is equal to  $2/3$ ; the change of the slope of  $\log_{10} R$  and

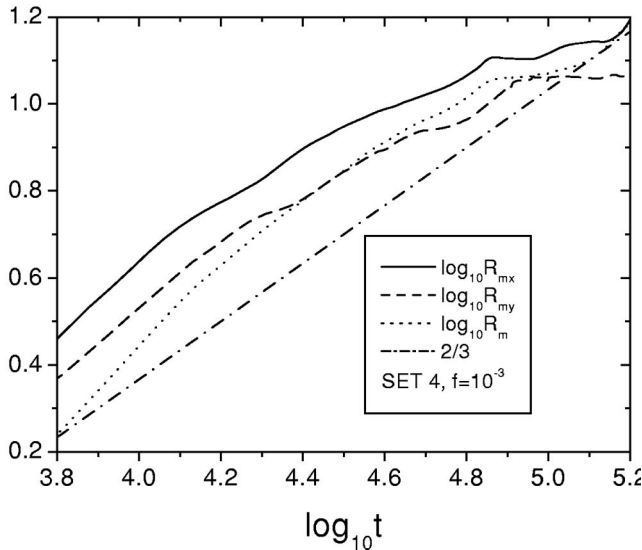
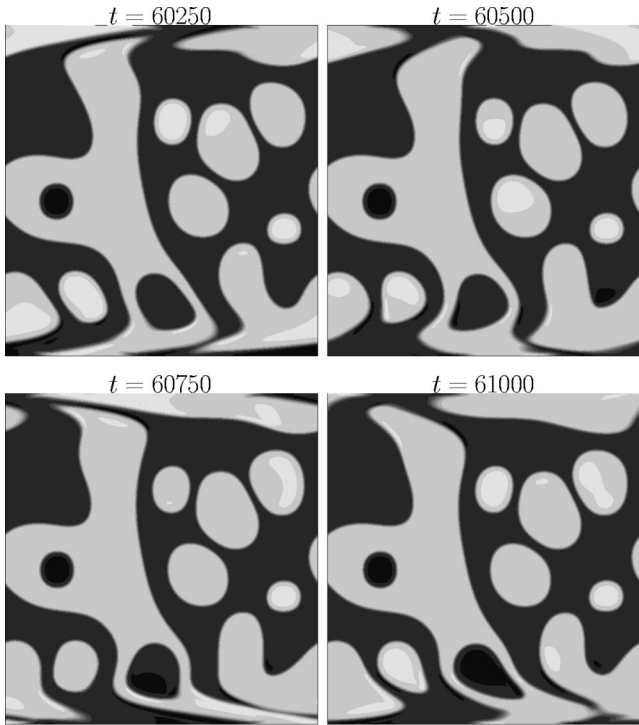


FIG. 7. Four configurations and size domain evolution for a run with parameter set 4 and  $f=10^{-3}$ . The configurations are taken at the four quarters of a period starting at  $t=60\,000$ . The quantities  $R_{mx}, R_{my}, R_m$  are the horizontal, vertical, spherically averaged domain sizes averaged over each period.

$\log_{10} R_x$  at  $\log_{10} t \sim 4.2$  is due to finite size effects which are more relevant in the direction of the flow. The behavior of  $R_y$  departs from the power law  $t^{2/3}$  at  $\log_{10} t \sim 3.5$ . This anisotropy is partially due to the presence of the walls which, even without flow, can inhibit the growth of domains in the vertical dimension at the bottom and at the top of the system. The morphology of the domains is also influenced by the shear velocity which is larger compared with the hydrodynamic velocities in the region close to the walls, see, Fig. 1. The

slightly anisotropic evolution at  $f=10^{-3}$  can be illustrated from the two configurations shown in Fig. 5 with the corresponding structure factors. The circular shape of the structure factor at  $t=1650$ , whose radius is of the order of the inverse of  $R(t)$ , reflects the isotropic configuration of the concentration field at this time. At  $t=5900$  the slight prevalence of the peaks at  $k_x=0$  corresponds to the presence of a recognizable amount of domains aligned with the flow close to the walls. In the following of this simulation the almost isotropic character is conserved as it has been checked looking at the configurations.

At the frequency  $f=10^{-4}$  the morphology of domains is more affected by the applied flow due to a bigger region of the system where the horizontal velocity is significantly larger than the typical hydrodynamic velocities measured along the vertical direction, see, Fig. 1. As a consequence, lamellas can be observed close to the walls while the growth keeps a more isotropic character in the middle of the system. Figure 6, at the frequency  $f=2 \times 10^{-5}$ , gives an example of this behavior with the evolution of the system shown for a whole period. Larger and more spherical domains can be observed in the middle of the system while, close to the walls, thin domains follow the direction of the flow and are subjected to a larger number of recombination and breakup processes. In this case and also at  $f=5 \times 10^{-6}$  it is not possible to speak of dynamical scaling since domains are distributed on different scales. However, it is worth to observe that the quantities  $R$  and  $R_y$  follow for a large interval of the evolution a power-law behavior with exponent  $2/3$ .

When the viscosity becomes larger, as for example in cases 2,4,5 of Table I, the evolution of the system without flow still corresponds to the inertial regime but the resulting shorter relaxation time  $T_R$  makes the presence of the flow in the bulk more effective with relevant consequences for the kinetics of phase separation. In particular, we have observed that the oscillatory flow can cause the interruption of the segregation process. This phenomenon, also reported in experiments [15,16], has been found in our simulations at different viscosities and in different growth regimes. An example of this flow-induced interruption of growth is shown in Fig. 7. The growth of  $R, R_x, R_y$  becomes very slow at  $\log_{10} t \sim 4.8$ . In Fig. 7 we also show a set of 4 configurations in a period at this time. We observe that the terminal regions of domains close to the walls follow with their movement the oscillation of the flow. The convection-induced movements inhibit the domain growth due to other mechanisms (diffusion or inertial), and the system appears for a certain interval of time in a sort of elastic stationary state. The size of domains where this phenomenon is first observed during the phase separation is found to be of the order of the average deformation  $2/(L-1) \int_0^{T/4} dt \int_0^{(L-1)/2} dy \gamma_0 y \cos(2\pi ft) = \gamma_0(L-1)/8\pi T$  in all cases considered.

### V. DIFFUSIVE GROWTH

In this section we consider the case where diffusion is the physical mechanism mainly responsible for phase separation. We will consider set 3 of parameters of Table I; the corresponding behavior of  $R(t)$  in quiescent conditions is shown

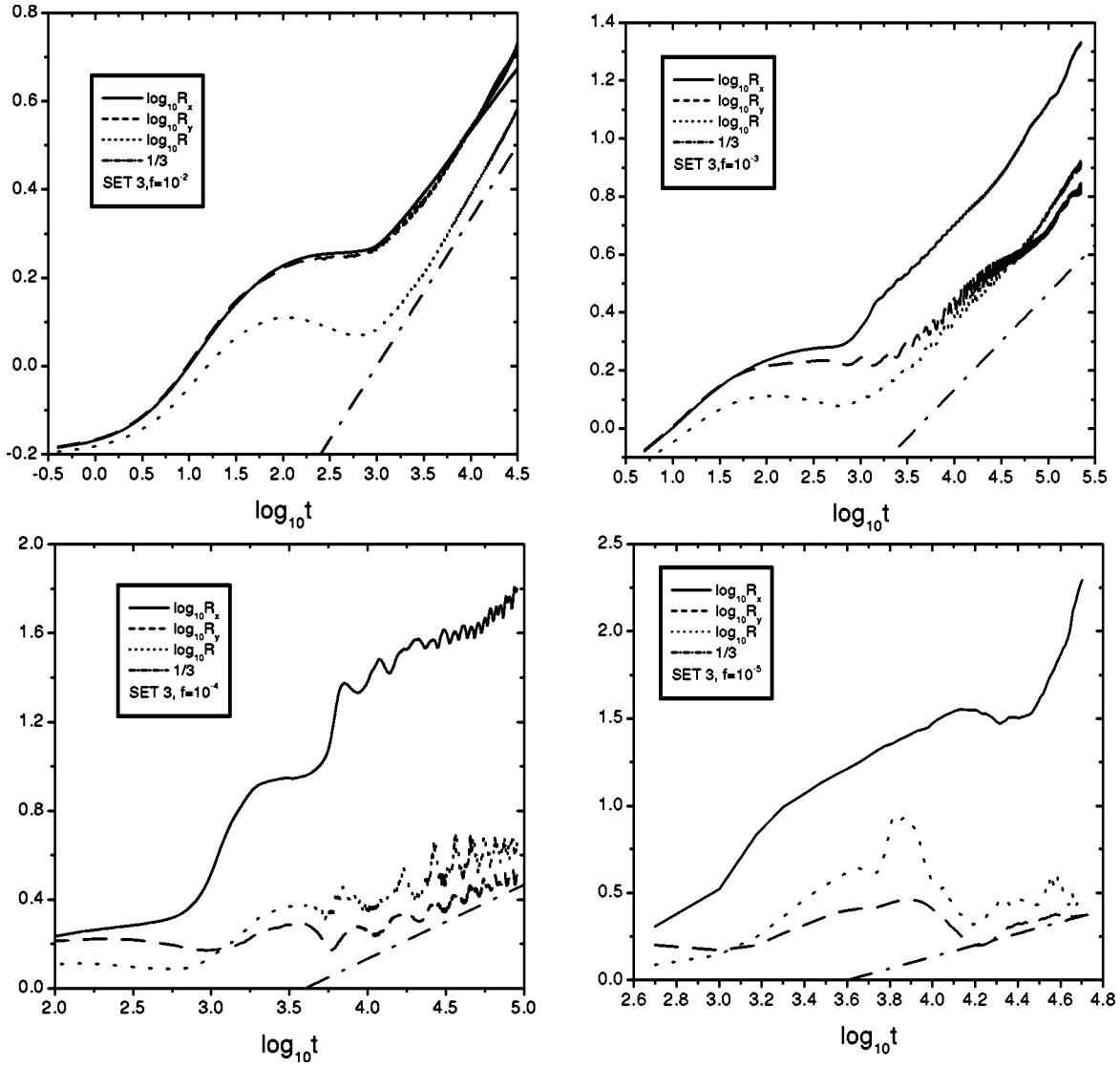


FIG. 8. Evolution of the horizontal, vertical, and spherically averaged domain size in double logarithmic scale. The straight dashed lines have the slope written in the insets.

in Fig. 3 with the value of the growth exponent given by  $\alpha = 0.35$ .

As in the previous cases also here the growth becomes more anisotropic when the frequency  $f$  decreases. However, due to a higher value of the viscosity,  $T_R$  is smaller and the effects of shear convection are more pronounced and observable already for  $f = 10^{-2}$ . Indeed, at this frequency, and also at  $f = 10^{-3}$ , as it can be seen in Fig. 8, at late times in the simulation,  $R_x$  and  $R$  grow faster than  $t^{1/3}$  with an effective exponent  $\alpha = 0.39$  at  $f = 10^{-2}$  and  $\alpha = 0.54$  at  $f = 10^{-3}$  for  $R(t)$ . This behavior can be understood by looking at the configurations of the concentration field. In Fig. 9 it is shown as an example at time  $t = 2250$  for  $f = 10^{-3}$ . Two different phases can be seen to coexist: lamellar ordered domains aligned with the flow close to the walls and the usual isotropic pattern of phase separation in the middle of the system. This coexistence is reflected in the shape of the structure factor which is circular with two peaks at  $k_x = 0$  corresponding to the horizontal lamellar domains. Then, as in diffusive

phase separation with steady shear, striped domains almost aligned with the flow grow in the flow direction faster than in the other directions with an exponent larger than  $1/3$ . In the case of Fig. 9, the effective exponents for  $R_x$  and  $R$ , which are quantities averaged over the whole system, will depend on the ratio between the volumes of the two coexisting phases.

By decreasing the frequency, the difference in the behavior of  $R_x$  and  $R_y$  becomes more pronounced, as it can be seen in Fig. 8 at  $f = 10^{-4}$  and  $f = 10^{-5}$ . The four configurations shown in Fig. 10 for the first period of the evolution at  $f = 10^{-4}$  exhibit elongated domains in the direction of the flow similar to those observed in the case of steady shear. This explains the big difference in the values measured for  $R_x$  and  $R_y$  in Fig. 8. Of course, also in this case the morphology of the domains is strictly related to the behavior of the horizontal velocity profiles shown in Fig. 1. We see that an almost regular triangular velocity profile occurs when the ratio between  $T_R$  and  $T$  is of order 1. Finally, a quantitative evalua-

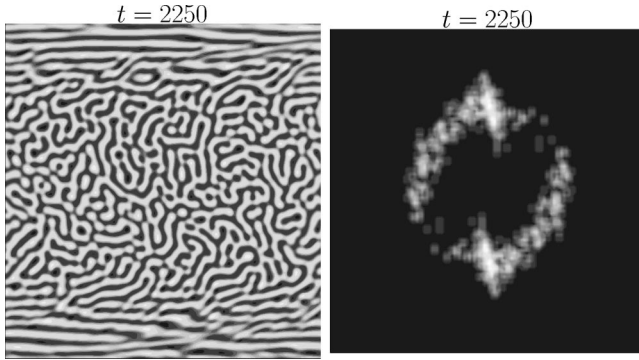


FIG. 9. A configuration with corresponding structure factor at  $t=2250$  in a simulation with parameter set 3 and  $f=10^{-3}$ . In the structure factor plot  $k_x$  (horizontal axis) and  $k_y$  (vertical axis) vary in the interval  $[-\pi/2, \pi/2]$ .

tion of the growth at the late stages of the simulation at  $f=10^{-4}$  can be better done by averaging the behavior of  $R_x$  and  $R_y$  over each period. This gives the exponents  $\alpha_x=0.65$  and  $\alpha_y=0.19$ . These results should be compared with the case of steady shear where a very slow growth is measured at late times in the shear direction.

## VI. STRESS BEHAVIOR

In this section we consider the behavior of the shear stress associated with the deformation of the domain pattern induced by the flow. The stress response  $\sigma_{xy}$  is calculated as the second momentum of the structure factor:

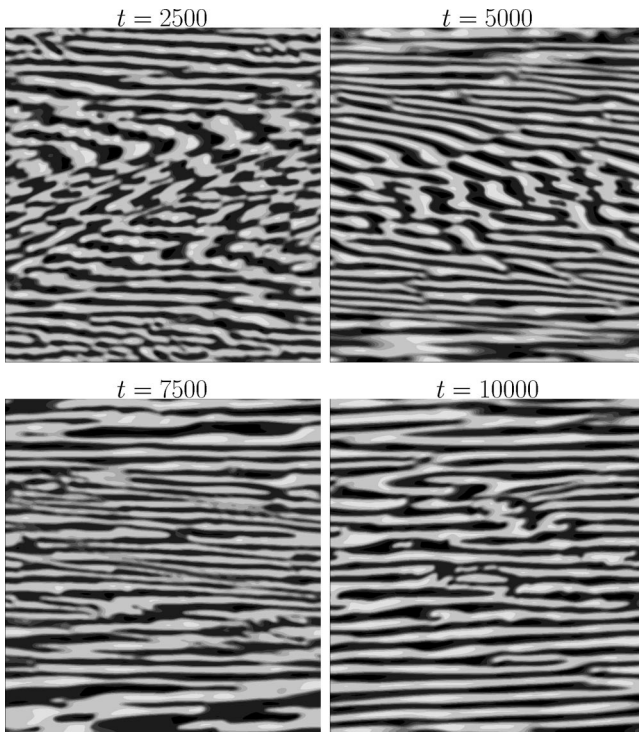


FIG. 10. Four configurations in a run with parameter set 3 and  $f=10^{-4}$ .

$$\sigma_{xy} = \int \frac{d\vec{k}}{(2\pi)^2} k_x k_y C(\vec{k}, t). \quad (29)$$

We first discuss a peculiar behavior that we find for the phase of the shear stress. We show in Fig. 11 the time evolution of  $\sigma_{xy}$  for the same frequencies and parameters of Fig. 4. For convenience, the velocity on the upper wall is also plotted in Fig. 11. We observe at the frequencies  $f=10^{-3}$  and  $f=10^{-4}$  a phase opposition between the stress and the velocity field imposed on the walls of the system. This unusual phase behavior can be explained by looking at the velocity profiles of Fig. 1 where we see that the velocity does never relax to the triangular profile but also assumes the “wrong” sign in proximity of the walls before the jump to the values imposed on the boundaries. Therefore, the stress follows the sign of the real velocity field in the system and this explains the “strange” phase behavior of the stress.

The above analysis is confirmed when we look in Fig. 12 at the case  $f=10^{-4}$  corresponding to the set 3 of parameters of Table I. In this case almost triangular profiles are obtained, see, Fig. 1, and indeed the stress is almost in phase with the velocity field on the walls.<sup>4</sup>

A more general feature of the behavior of the shear stress can be observed in all the cases shown. We see that the initial evolution of the stress is always characterized by the presence of a peak which can be eventually followed by other large oscillations. This is clear from the inset of Fig. 11 for  $f=10^{-3}$  where two overshoots modulated by small oscillations due to the velocity field can be observed. The phenomenon is enhanced at  $f=10^{-4}$  and  $f=2 \times 10^{-5}$  where the time between successive peaks is of the same order of the period of the applied flow and is also present at  $f=5 \times 10^{-6}$  confirming that its origin is independent of the oscillations of the flow. Indeed, for the latter mentioned frequency, we observe overshoots of  $\sigma_{xy}$  while the phase of the applied flow has not changed sign. Similar phenomena are also observed in Fig. 12.

Overshoots of the shear stress have been reported in experiments of phase separation with steady shear [56] and have also been found in simulations [12,13,38]. The phenomenon is interpreted, as due to an initial stretching of the domains in the direction of the flow to which it corresponds to an increase of  $\sigma_{xy}$ . At a certain point the deformation cannot be sustained by the surface tension and the domains start to break evolving in less stretched configurations. This occurs in correspondence with a maximum of  $\sigma_{xy}$ . Then the system becomes more isotropic but, after that a minimum in  $\sigma_{xy}$  is reached, elastic energy is again stored due to the deformations and another overshoot of  $\sigma_{xy}$  can be observed.

The above considerations can be extended also to our case with further complications due to the flow oscillations. In particular, at frequencies of the order of the inverse of time

<sup>4</sup>A complete analysis of the viscoelastic properties of phase separating binary mixtures, with the evaluation of the elastic and viscous parts of the stress response, is beyond the purposes of this work.

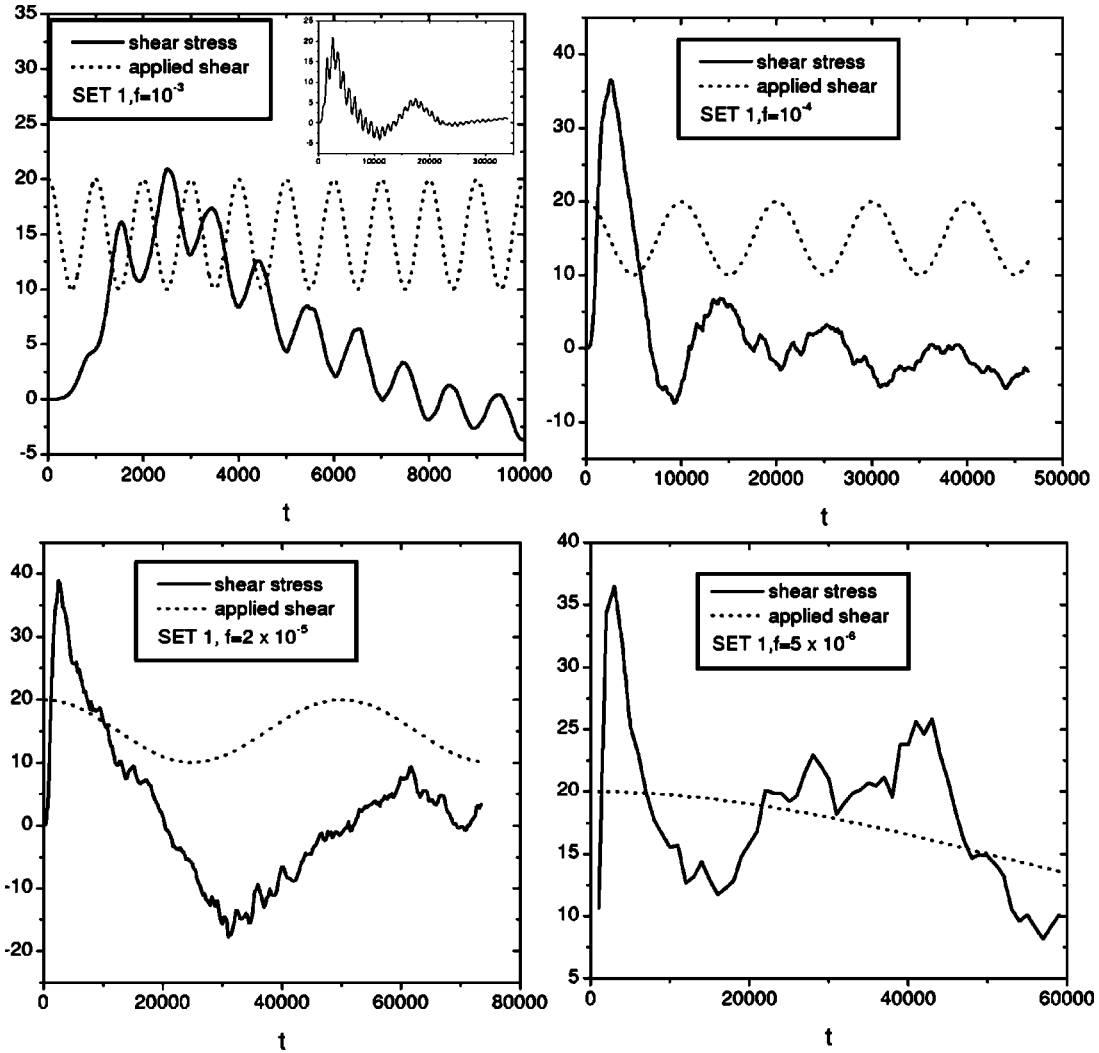


FIG. 11. Behavior of the shear stress compared with the velocity on the upper wall. In the case with frequency  $f=10^{-3}$  the overall behavior is shown in the inset and only the initial evolution is plotted in the main frame. The plot of the velocity is translated along the vertical axis for graphical convenience; units are arbitrary for both the quantities.

between two overshoots of  $\sigma_{xy}$ , the relaxation or the stretching phenomena discussed above in the case of steady shear are greatly influenced by the flow oscillations. For example, in the case  $f=2 \times 10^{-5}$  of Fig. 11, the relaxation after the first maximum of  $\sigma_{xy}$  occurs in correspondence with the change of sign of the imposed velocity and, therefore, one can think that the decreasing of the stress is mainly due to the reversed sign of the deformations than to breaking processes in the domain pattern. This results in two very well shaped overshoots than those occurring in the case  $f=5 \times 10^{-6}$  which resembles what would occur with steady shear.

## VII. CONCLUSIONS

In this work we have studied the behavior of phase separating binary mixtures subjected to oscillatory shear for different viscosities and frequencies of the applied flow. The existence of different physical mechanisms operating in phase separation, the anisotropic effects induced by the flow, and a finite relaxation time  $T_R$  for the triangular velocity

profile contribute to giving rise to a very rich phenomenology. In particular, the role of viscosity is fundamental because both the occurrence of inertial or diffusive growth and the time  $T_R$  depend on the viscosity.

In this complex framework we found that the ratio  $T_R/T$  can be used as a convenient parameter for measuring the effects of the applied flow. At low viscosity and high frequency, for example, when the ratio  $T_R/T$  is larger than 1, the effects of the shear are limited to a region close to the walls of the system, while in the bulk the growth is isotropic as in the case without applied flow. Actually, the most interesting phenomena can be observed when the above ratio becomes of order 1. Different phases, with lamellar order in regions close to the walls and isotropically oriented domains in the central part of the system, have been observed to coexist and evolve together in this case. For particular values of the frequency and viscosity we have also observed the interruption or slowing of the process of segregation: interfaces are convected successively in opposite directions with the net effect of inhibiting any other growth mechanism, at least for a significantly large time interval in simulations. Finally,

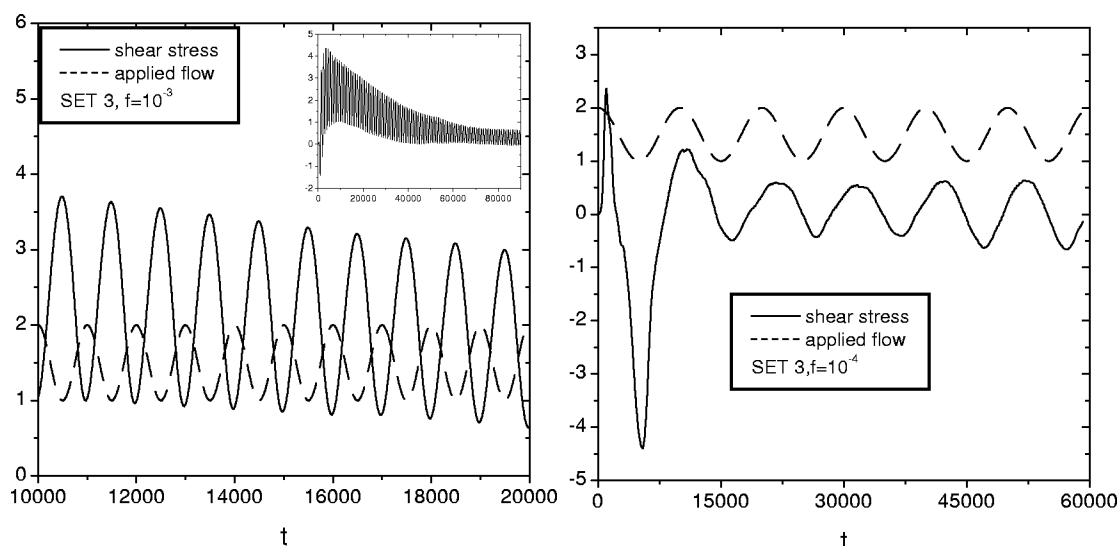


FIG. 12. Shear stress and applied flow as in the previous figure, now for cases with parameter set 3. In the case with frequency  $f = 10^{-3}$  the overall behavior is shown in the inset while in the main frame the evolution in the time interval  $[10\,000, 20\,000]$  is plotted. The plot of the velocity is translated along the vertical axis for graphical convenience; units are arbitrary for both the quantities.

for values of the ratio  $T_R/T$  much less than 1, the domains grow with lamellar morphology everywhere in the system as in the case of steady flow.

The question of the existence of power-law behavior for the domain size  $R_x, R_y$  has a definite answer only in some cases. For sufficiently high frequencies the power-law behavior of the case without flow, inertial or diffusive depending on the viscosity, is generally recovered. At lower frequencies, when different scales for the size of domains are observed at the same time in the system, it is not possible to speak of dynamical scaling; however, the quantities  $R_x, R_y$  that we measure still give information about the growth behavior. We can note that in the limit of very low frequencies we have not found any signal of a stationary state with the size of domains reaching or tending to a finite value. Actu-

ally, we have measured effective growth exponent in the shear direction less than the expected values in the absence of flow which indicate a continuation of the phase separation also at the late times of our simulations. This could be an indication for the case with steady shear suggesting a growth of domains also at asymptotic times.

We hope that our analysis of the segregation process in binary mixtures under oscillatory shear will stimulate a more systematic experimental investigation of these systems. A natural continuation of this study will be its extension to the three-dimensional case.

#### ACKNOWLEDGMENT

A.L. acknowledges INFM for partial support.

- 
- [1] See, e.g., R.G. Larson, *The Structure and Rheology of Complex Fluids* (Oxford University Press, New York, 1999).
- [2] A. Onuki, *J. Phys.: Condens. Matter* **9**, 6119 (1997).
- [3] T. Hashimoto, K. Matsuzaka, E. Moses, and A. Onuki, *Phys. Rev. Lett.* **74**, 126 (1995).
- [4] J. Lauger, C. Laubner, and W. Gronski, *Phys. Rev. Lett.* **75**, 3576 (1995).
- [5] S.F. Bates, *Science* **251**, 898 (1991).
- [6] G. Fredrickson, *J. Rheol.* **38**, 1045 (1994).
- [7] A.N. Morozov, A.V. Zvelindovsky, and J.G.E.M. Fraaije, *Phys. Rev. E* **64**, 051803 (2001); A.V. Zvelindovsky, G.J.A. Sevink, B.A.C. van Vlimmeren, N.M. Maurits, and J.G.E.M. Fraaije, *ibid.* **57**, R4879 (1998).
- [8] F. Corberi, G. Gonnella, and A. Lamura, *Phys. Rev. E* **66**, 016114 (2002).
- [9] J.D. Gunton, M. San Miguel, and P.S. Sahni, in *Phase Transitions and Critical Phenomena*, edited by C. Domb and J.L. Lebowitz (Academic, New York, 1983).
- [10] K. Migler, C. Liu, and D.J. Pine, *Macromolecules* **29**, 1422 (1996).
- [11] F. Corberi, G. Gonnella, and A. Lamura, *Phys. Rev. Lett.* **81**, 3852 (1998).
- [12] F. Corberi, G. Gonnella, and A. Lamura, *Phys. Rev. Lett.* **83**, 4057 (1999).
- [13] Feng Qiu, Hongdong Zhang, and Yuliang Yang, *J. Chem. Phys.* **109**, 1575 (1998).
- [14] R.I. Tanner, *Engineering Rheology* (Clarendon, Oxford, 1988).
- [15] D. Beysens and F. Perrot, *J. Phys. (France) Lett.* **45**, L31 (1984).
- [16] A.H. Krall, J.V. Sengers, and K. Hamano, *Phys. Rev. E* **48**, 357 (1993).
- [17] K. Matsuzaka, H. Jinnai, T. Koga, and T. Hashimoto, *Macromolecules* **30**, 1146 (1997).
- [18] F. Corberi, G. Gonnella, and A. Lamura, *Phys. Rev. E* **61**, 6621 (2000).

- [19] A. Malevanets and J.M. Yeomans, *Faraday Discuss.* **112**, 237 (1999).
- [20] H. Schlichting, *Boundary Layer Theory* (McGraw Hill, New York, 1979).
- [21] R. Benzi, S. Succi, and M. Vergassola, *Phys. Rep.* **222**, 145 (1992).
- [22] S. Chen and G.D. Doolen, *Annu. Rev. Fluid Mech.* **30**, 329 (1998).
- [23] S. Succi, *The Lattice Boltzmann Equation* (Oxford University Press, New York, 2001).
- [24] J.M. Yeomans, *Annu. Rev. Comput. Phys.* **VII**, 61 (2000).
- [25] M.E. Cates, V.M. Kendon, P. Bladon, and J.C. Desplat, *Faraday Discuss.* **112**, 1 (1999).
- [26] W.R. Osborn, E. Orlandini, M.R. Swift, J.M. Yeomans, and J.R. Banavar, *Phys. Rev. Lett.* **75**, 4031 (1995).
- [27] H. Furukawa, *Adv. Phys.* **34**, 703 (1985).
- [28] A.J. Bray, *Adv. Phys.* **43**, 357 (1994).
- [29] I.M. Lifshitz and V.V. Slyozov, *J. Phys. Chem. Solids* **19**, 35 (1961).
- [30] E.D. Siggia, *Phys. Rev. A* **20**, 595 (1979).
- [31] N.P. Rapapa and A.J. Bray, *Phys. Rev. Lett.* **83**, 3856 (1999).
- [32] D.H. Rothman, *Europhys. Lett.* **14**, 337 (1991).
- [33] P. Padilla and S. Toxvaerd, *J. Chem. Phys.* **106**, 2342 (1997).
- [34] A. Lamura and G. Gonnella, *Physica A* **294**, 295 (2001).
- [35] G. Gonnella, E. Orlandini, and J.M. Yeomans, *Phys. Rev. Lett.* **78**, 1695 (1997).
- [36] A.J. Wagner and J.M. Yeomans, *Phys. Rev. E* **59**, 4366 (1999).
- [37] M. Doi and T. Ohta, *J. Chem. Phys.* **95**, 1242 (1991).
- [38] T. Ohta, H. Nozaki, and M. Doi, *Phys. Lett. A* **145**, 304 (1990); *J. Chem. Phys.* **93**, 2664 (1990).
- [39] E. Orlandini, M.R. Swift, and J.M. Yeomans, *Europhys. Lett.* **32**, 463 (1995).
- [40] M.R. Swift, E. Orlandini, W.R. Osborn, and J.M. Yeomans, *Phys. Rev. E* **54**, 5041 (1996).
- [41] P. Bhatnagar, E.P. Gross, and M.K. Krook, *Phys. Rev.* **94**, 511 (1954).
- [42] H. Chen, S. Chen, and W. Matthaeus, *Phys. Rev. A* **45**, R5339 (1992).
- [43] J.S. Rowlinson and B. Widom, *Molecular Theory of Capillarity* (Clarendon Press, Oxford, 1982).
- [44] A.J.M. Yang, P.D. Fleming, and J.H. Gibbs, *J. Chem. Phys.* **64**, 3732 (1976).
- [45] R. Evans, *Adv. Phys.* **28**, 143 (1979).
- [46] Y.H. Qian, D. d'Humieres, and P. Lallemand, *Europhys. Lett.* **17**, 419 (1992).
- [47] Y.H. Qian and S.A. Orszag, *Europhys. Lett.* **21**, 255 (1993).
- [48] S. Chapman and T. Cowling, *The Mathematical Theory of Non-uniform Gases* (Cambridge University Press, Cambridge, 1970).
- [49] P. Lavallée, J. Boon, and A. Noullez, *Physica D* **47**, 233 (1991).
- [50] R. Cornubert, D. d'Humieres, and D. Levermore, *Physica D* **47**, 241 (1991).
- [51] J.C. Desplat, I. Pagonabarraga, and P. Bladon, *Comput. Phys. Commun.* **134**, 273 (2001).
- [52] A.J. Briant, P. Papatzacos, and J.M. Yeomans, *Philos. Trans. R. Soc. London* **360**, 485 (2002).
- [53] V.M. Kendon, J.C. Desplat, P. Bladon, and M.E. Cates, *Phys. Rev. Lett.* **83**, 576 (1999); V.M. Kendon, M.E. Cates, J.C. Desplat, I. Pagonabarraga, and P. Bladon, *J. Fluid Mech.* **440**, 147 (2001).
- [54] R.S. Maier and R.S. Bernard, *Int. J. Mod. Phys. C* **8**, 747 (1997).
- [55] A.J. Wagner and J.M. Yeomans, *Phys. Rev. Lett.* **80**, 1429 (1998).
- [56] A.H. Krall, J.V. Sengers, and K. Hamano, *Phys. Rev. Lett.* **69**, 1963 (1992).